



Calculation of mass transfer coefficients for corrosion prediction in two-phase gas-liquid pipe flow

Luciano D. Paolinelli*, Srdjan Nesic

Institute for Corrosion and Multiphase Technology, Department of Chemical and Biomolecular Engineering, Ohio University, Athens OH, 45701, USA



ARTICLE INFO

Article history:

Received 13 May 2020

Revised 9 October 2020

Accepted 1 November 2020

Available online 16 November 2020

Keywords:

Gas-liquid flow
mass transfer
flow patterns
mechanistic modeling, corrosion

ABSTRACT

Internal corrosion in industrial environments involving gas-liquid flow can be a serious concern. For example, in the oil and gas industry, corrosive water phase is usually transported in pipes along with liquid and/or gas hydrocarbon phases. These gas-liquid flows develop complex flow patterns where the liquid phase can distribute in quite different ways (as stratified layers, intermittent slugs, annular film, etc.) depending on the gas and liquid flow rates and pipe inclination. In these circumstances, the water phase can flow at very high velocities leading to high turbulence and mass transfer rates that can accelerate corrosion of the metallic pipe surface. In general, proper prediction of corrosion rates via mechanistic electrochemical models requires the knowledge of the mass transfer rate of corrosive species in the aqueous phase. There are very few studies in the open literature that show specific experimental data or propose ways to compute mass transfer rates in gas-liquid flow; particularly, for large pipe diameters. The present study introduces a methodology for the estimation of mass transfer rates in gas-liquid flow via the Chilton-Colburn analogy and near-wall eddy diffusivity distribution based on the mechanistic gas-liquid flow modeling. The proposed mechanistic models cover a wide range of fluid's properties and flow rates, different flow patterns and pipe inclinations, and show good agreement with mass transfer experimental data from large-scale gas-liquid flow.

© 2020 Elsevier Ltd. All rights reserved.

1. Introduction

Internal corrosion can be an important problem in an industry that deals with production and/or transportation of liquid and gas phases. In the oil and gas industry, oil is usually produced and transported by pipelines accompanied by different amounts of gas and some corrosive water (carrying dissolved CO_2 and H_2S). Conversely, pipelines carrying natural gas usually have some light hydrocarbon and water condensation occurring in the presence of acid gases CO_2 and H_2S . In both scenarios, a gas-liquid mixture is transported via mild steel pipelines over long distances. Any contact of the corrosive water with the inner pipe wall may lead to corrosion problems.

In gas-liquid flows a wide variety of flow patterns can develop, in which the liquid phase distributes in different ways. For example, in horizontal flow, relatively low superficial liquid velocities (liquid flow rates), and low to moderate superficial gas velocities

(gas flow rates) lead to stratified flow with gas flowing at the top and liquid at the bottom of the pipe with a smooth or wavy gas liquid interface ("ST" pattern in Fig. 1). The operating region for stratified flow drastically narrows even for very small upward inclination angles (e.g., ~ 1 degree) favoring the occurrence of intermittent flow pattern such as slug flow [1].

Slug flow occurs at moderate superficial liquid velocities and a wide range of superficial gas velocities, as shown as "SL" pattern in Fig. 1. Very high liquid velocities can be found in this flow pattern since the velocity of liquid slugs is approximately equal to the sum of superficial velocities of the liquid and gas phases. In horizontal flow, the velocity of the liquid film, moving in the gas pocket zones between the liquid slugs, is relatively low compared to the velocity of the liquid slugs themselves. However, liquid film velocities can be higher in upward inclined and vertical flows where the liquid film can move counter current while the gas pockets flow with the main stream.

When superficial gas velocities are high and the liquid holdup is not high enough to bridge the entire pipe cross-section to produce liquid slugs, the gas phase flows through the core of the pipe and entrains liquid droplets which can be simultaneously deposited all around the pipe circumference, producing an annular liquid film. This flow pattern is called annular mist ("AM" pattern in Fig. 1).

* Corresponding author: Luciano D. Paolinelli, Institute for Corrosion and Multiphase Technology, Department of Chemical & Biomolecular Engineering, Ohio University, 342 W. State Street, Athens OH 45701, T: 740.593.9612, F: 740.593.994; E-mail:

E-mail address: paolinel@ohio.edu (L.D. Paolinelli).

Notations

A	cross-sectional area of the pipe, m^2
c	concentration of a given species, Mol/m^3
c_b	concentration of a given species in the bulk fluid, Mol/m^3
c_w	concentration of a given species at the pipe wall, Mol/m^3
C_f	constant in equation (A.12), dimensionless
C_t	constant for the eddy diffusivity function, dimensionless
C_o	distribution parameter of the drift-flux model, dimensionless
C_1, C_2	constants in equation (13)
c'	concentration fluctuations of a given species, Mol/m^3
D	molecular diffusion coefficient of a given species, m^2/s
D_t	turbulent mass diffusion coefficient, m^2/s
d	pipe diameter, m
d_{gf}	hydraulic diameter of the gas flow, m
d_{lf}	hydraulic diameter of the liquid film flow, m
E	entrained liquid fraction, dimensionless
f	Fanning friction factor, dimensionless
f_{gf}	friction factor for the gas layer, dimensionless
f_i	friction factor for the gas-liquid interface, dimensionless
f_{lf}	friction factor for the liquid film flow, dimensionless
f_{ls}	friction factor for the gas-liquid flow in the slug cylinder, dimensionless
f_m	friction factor for the gas-liquid mix flow, dimensionless
g	gravitational acceleration, m/s^2
IP	oil-water phase inversion point, dimensionless
k_m	mass transfer coefficient, m/s
k_{mf}	mass transfer coefficient at the liquid film, m/s
k_{ms}	mass transfer coefficient at the slug cylinder, m/s
n	exponent in equations (1), (2) and (10), dimensionless
n_f	exponent in equation (A.12), dimensionless
N	mass flux of a given species, $Mol/(m^2.s)$
N_w	mass flux of a given species at the pipe wall, $Mol/(m^2.s)$
r_{cyl}	radius of the rotating cylinder, m
R	chemical reaction source term, $Mol/(m^3.s)$
Re	Reynolds number, dimensionless
Re_{cyl}	Reynolds number of the rotating cylinder, dimensionless
Re_g	Reynolds number of the gas flow, dimensionless
Re_i	Reynolds number based on the velocity of the gas-liquid interface, dimensionless
Re_{lf}	Reynolds number of the liquid film flow, dimensionless
Re_m	Reynolds number of the mixture gas-liquid flow, dimensionless
S_{gf}	pipe perimeter wetted by gas, m
S_i	perimeter of the gas-liquid interface, m
S_{lf}	pipe perimeter wetted by liquid, m
Sc	Schmidt number, dimensionless
Sh	Sherwood number, dimensionless
Sh_{cyl}	Sherwood number of the rotating cylinder, dimensionless
u	fluid velocity, m/s

u_b	Taylor bubble velocity, m/s
u_{cyl}	velocity of the rotating cylinder surface, m/s
u_{gf}	velocity of the gas flow, m/s
u_i	velocity of the gas-liquid interface, m/s
u_l	velocity of the liquid flow, m/s
u_{lf}	velocity of the liquid film, m/s
u_m	gas-liquid mixture velocity, m/s
u_{sg}	superficial gas velocity, m/s
u_{sl}	superficial liquid velocity, m/s
u_{so}	superficial oil velocity, m/s
u_{sw}	superficial water velocity, m/s
u_t	velocity of the liquid slug front, m/s
u^*	friction velocity of the liquid flow, m/s
u^*_{lf}	friction velocity of the liquid film, m/s
u^*_{ls}	friction velocity of the liquid slug, m/s
\bar{u}^*	average liquid friction velocity for slug flow, m/s
u'	liquid velocity fluctuations in the y direction, m/s
y	normal coordinate respect to the pipe wall, m
y^+	dimensionless distance from the pipe wall

Greek letters

α_{gf}	holdup of gas or gas with entrained liquid droplets, dimensionless
α_{gr}	gas holdup of the flow of gas with entrained liquid droplets, dimensionless
α_l	liquid holdup, dimensionless
α_{lf}	liquid film holdup, dimensionless
α_{ls}	liquid slug holdup, dimensionless
β	pipe inclination angle from the horizontal, radians
β_s	relative slug length, dimensionless
δ	thickness of the diffusion boundary layer, m
ε_w	volumetric fraction of water based on total liquid volume, dimensionless
μ_g	gas dynamic viscosity, Pa.s
μ_{gf}	dynamic viscosity of the gas with entrained liquid droplets, Pa.s
μ_l	liquid dynamic viscosity, Pa.s
μ_{lm}	dynamic viscosity of the oil-water mixture, Pa.s
μ_{ls}	dynamic viscosity of the liquid slug, Pa.s
μ_m	dynamic viscosity of the gas-liquid mixture, Pa.s
μ_o	oil dynamic viscosity, Pa.s
μ_w	water dynamic viscosity, Pa.s
ν_l	liquid kinematic viscosity, m^2/s
ρ_g	gas density, kg/m^3
ρ_{gf}	density of the gas with entrained liquid droplets, kg/m^3
ρ_l	liquid density, Pa.s
ρ_{lm}	oil-water mixture density, kg/m^3
ρ_{ls}	liquid slug density, kg/m^3
ρ_m	gas-liquid mixture density, kg/m^3
ρ_o	oil density, kg/m^3
ρ_w	water density, kg/m^3
σ	gas-liquid surface tension, N/m
τ_{gf}	wall shear stress of the gas bubble in slug flow, Pa
τ_i	shear stress at the gas-liquid interface, Pa
τ_l	wall shear stress due to the liquid flow, Pa
τ_{lf}	wall shear stress of the liquid film in slug flow, Pa
τ_{ls}	wall shear stress of the liquid slug, Pa
ω	rotational speed of the rotating cylinder, radians/s

Acronyms

AM	Annular mist flow pattern
CFD	Computational Fluids Mechanics
DB	Dispersed bubble flow pattern

MT	Mass transfer
RC	Rotating cylinder
SL	Slug flow pattern
ST	Stratified flow pattern

For high superficial liquid velocities, the gas phase is fully entrained and dispersed as bubbles in the liquid phase, which is the flow pattern indicated as “DB” in Fig. 1.

In some of the gas-liquid flow patterns described above (e.g., SL and AM) very high liquid velocities can develop, when compared to typical single-phase water flow or two-phase oil-water flows. These high liquid velocities lead to high wall shear stresses and high mass transfer (MT) rates that can significantly accelerate corrosion of internal pipe surfaces.

Mechanistic models used to predict corrosion rate in these types of scenarios are based on modeling the kinetics of electrochemical reactions occurring at the pipe surface; e.g., oxidation of iron and reduction of hydronium ions, which are in balance. The hydronium ion reduction reaction is often limited by the rate of MT of this corrosive species from the bulk to the metal surface, where it is consumed in the corrosion process. Therefore, it is crucial to be able to calculate MT rates with reasonable accuracy, in order to obtain a good prediction of corrosion rates [2,3]. Similar mass transfer limited electrochemical kinetics is found in other types of corrosion where the corrosive species is dissolved oxygen.

There are other types of corrosion scenarios where MT plays a crucial role. For example, high MT of corrosion products away from the metal surface can make it harder to form corrosion product layers on the metal surface. Corrosion products are species produced by the anodic dissolution of metal, for example, in mild steel corrosion – the ferrous ions, Fe^{2+} , which are an important building block when it comes to forming protective corrosion product layers, such as iron carbonate or iron sulfide. Flow enhanced MT can also be a controlling factor in chemical dissolution of existing protective corrosion product layers, which can be significantly enhanced by MT that moves the products of dissolution away from the surface, thereby allowing for the dissolution process to proceed at a higher rate.

Mass transport from a bulk liquid phase to a solid pipe wall in multiphase gas-liquid flow have been studied previously, mainly by means of electrochemical techniques such as the measurements of limiting currents using inert electrodes flush mounted at the inner pipe surface [4–9]. Only a few studies were performed in pipes with relatively large diameter (e.g., 0.1m) which are more representative of the flows encountered in the field [4,7,8]. Regarding the calculation of MT rates in large scale gas-liquid pipe flow, there have been attempts to build correlations similar to the one proposed by Berger and Hau [10] for single-phase pipe flow [7,11]. Those models were not mechanistic in nature and oversimplified the link between the wall shear stress and MT rate without covering all relevant flow patterns.

The objective of this study is to introduce a sound methodology for the estimation of MT rates in multiphase gas-liquid flow. Two different approaches are proposed, one for calculation of integral MT coefficients in turbulent flow based on the Chilton-Colburn analogy between momentum and MT. The second more elaborate approach also uses momentum and MT similarity in turbulent flow to calculate the distribution of eddy diffusivity across the boundary layer. Both approaches are linked to mechanistic gas-liquid flow modeling to obtain the key liquid flow parameters (liquid velocity and wall shear stress) in the various flow patterns. Resulting MT calculations are discussed and compared with available experimental data obtained in large-scale gas-liquid flow with different flow patterns.

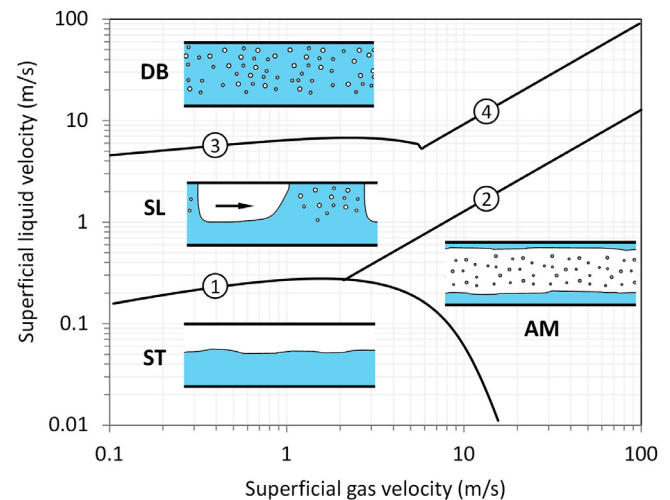


Fig. 1. Calculated gas-liquid flow map. AM: Annular mist flow, DB: Dispersed bubble flow, SL: Slug/intermittent flow, ST: Stratified flow. Horizontal flow, $d = 0.1$ m, $\rho_l = 1000$ kg/m³, $\mu_l = 1$ mPa.s, $\rho_g = 10$ kg/m³, $\mu_g = 0.018$ mPa.s.

2. Momentum and mass transfer analogy

As stated above, there are very few attempts found in the open literature to experimentally and theoretically establish MT correlations for various multiphase gas-liquid flow patterns. On the other hand, the literature covering hydrodynamic models for calculation of the key characteristics of multiphase flow, such as: pressure drop, holdup, flow pattern, distribution of phases, wall shear stress, etc., is plentiful and reasonably accurate models have long been established. This body of knowledge in multiphase hydrodynamics can be engaged by introducing widely used analogies between momentum and MT. These analogies are based on the fundamental similarity between the two transport mechanisms, which results in very similar forms of the transport equations for momentum and MT. Among the different analogies (such as Reynolds analogy, Prandtl–Taylor analogy, etc.), the Chilton–Colburn analogy proved to be the most accurate.

2.1. Chilton–Colburn analogy

MT coefficient in fully developed turbulent boundary layer flow can be related to the wall shear stresses via the Chilton–Colburn analogy [12], as shown by the following relationship between dimensionless quantities:

$$Sh = \left(\frac{f}{2} \right)^n Re Sc^{1/3} \quad (1)$$

where $Sh = k_m d/D$ is the Sherwood number, $f = \tau/(\rho u^2/2)$ is the Fanning friction factor, τ is the wall shear stress, u is the mean velocity of the fluid, $Re = ud/\nu$ is the Reynolds number, $Sc = \nu/D$ is the Schmidt number, $\nu = \mu/\rho$ is the fluid kinematic viscosity, μ is the fluid dynamic viscosity, ρ is the fluid density, D is the diffusion coefficient of a given species in the given fluid, k_m is the MT coefficient, d is a characteristic length (for single phase pipe flow it is the internal pipe diameter). The exponent n is equal to 1, according to the original work of Chilton and Colburn [12]. It was later suggested by some authors that the exponent n can be between 1 and 0.5 [10,13,14]. For cases where $Sc = 1$, the original Chilton–Colburn correlation (1) simplifies to the Reynolds analogy. However, for aqueous species typical seen in corrosion, the Sc is of the order of $10^2 - 10^3$ or even higher, hence the Chilton–Colburn analogy needs to be used.

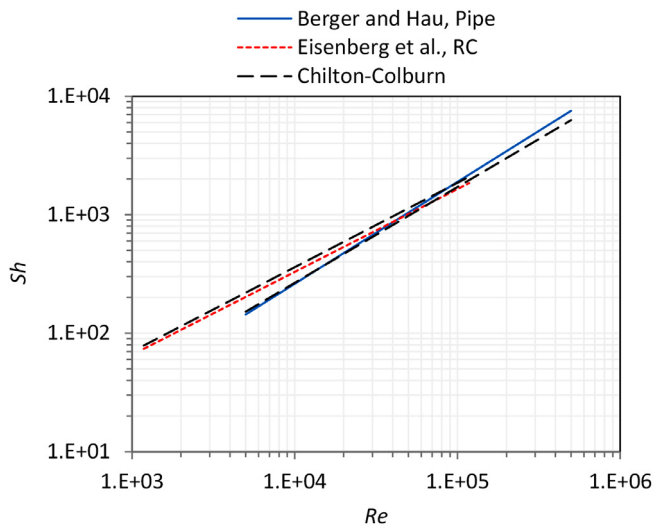


Fig. 2. Sherwood numbers for pipe and rotating cylinder (RC) calculated using the Chilton-Colburn analogy, equation (1) compared to well-established mass transfer correlation of Berger and Hau for turbulent straight pipe flow and Eisenberg et al. for turbulent rotating cylinder flow; $Sc = 200$, $d_{\text{pipe}} = 0.1$ m, $2r_{\text{cyl}} = 0.015$ m, $\rho = 1000$ kg/m³, $\mu = 1$ mPa·s.

The MT coefficient can be calculated directly from (1) as:

$$k_m = \left(\frac{\tau}{\rho u^2} \right)^n u Sc^{-2/3} \quad (2)$$

The convenience of equation (2) is in that as long as the wall shear stress and the mean flow velocity are known – the MT coefficient can be estimated, regardless of the flow geometry or flow pattern (e.g., single-phase or multiphase pipe flow, rotating cylinder flow, turbulent jet impingement, etc.). This is illustrated in Fig. 2 that shows the Sherwood numbers for hydraulically smooth pipe and rotating cylinder flows calculated by the Chilton-Colburn analogy, equation (1) (black dashed lines) using the friction factors described in the Appendix (equations (A.1) and (A.3), respectively), and compares them with the Sherwood numbers calculated using the widely accepted Berger and Hau [10] and Eisenberg et al. [15] correlations for turbulent straight pipe flow and rotating cylinder flow (equations (A.2) and (A.6), respectively, see Appendix). An exponent of $n = 0.96$ is found to be the most appropriate to estimate the MT characteristics for both flow geometries in the range $100 \leq Sc \leq 1000$ with an average absolute error $\leq 10\%$.

2.2. Near-wall eddy diffusivity distribution

There are situations where integral MT coefficients cannot be used. Some examples are: disturbed flow geometries where the boundary layer is not fully developed and the MT rates vary across the surface [16–23]; another example is MT in so called reacting boundary layers, i.e. when multi-species MT between the bulk and the solid surface is accompanied by simultaneous chemical reaction between those species [2,24–27]; the case of MT of charged (ionic) species in the presence of electrical fields [28–31]. In all those cases it is more complicated to calculate the MT rates. One cannot assume a linear variation of the concentration between the bulk and the solid surface and use an integral MT coefficient, such as for example the one calculated by using equation (2). Instead, more elaborate models are needed that can resolve species concentrations profiles throughout the MT boundary layer, by including all the relevant physics: mass transfer by molecular diffusion, turbulent convection and electromigration as well as the effect of homogenous and heterogenous (electro)chemical reactions.

When it comes to turbulent convection, the influence of turbulent eddies penetrating into the viscous sublayer on MT is very significant, particularly at high Sc number such as the ones found in aqueous corrosion systems. In order to model this effect, one must quantify the turbulent convection of species as a function of the distance from the solid surface. In steady state turbulent flow, in the boundary layer, where the mean flow is parallel to the surface, the mass flux of a given species in the direction (y) normal to a surface can be written as having two main contributions: molecular diffusion and turbulent convection¹:

$$N = D \frac{\partial c}{\partial y} + \overline{u'c'} \quad (3)$$

where c is the time averaged concentration, c' is the concentration fluctuation, and u' is the flow velocity fluctuation in the y direction. The turbulent convective term $\overline{u'c'}$ can be calculated by using advanced computational fluid dynamic (CFD) codes or replaced by a diffusion-like term by using the concept of eddy diffusivity, which is added to the molecular diffusivity, to get the mass flux:

$$N = (D + D_t) \frac{\partial c}{\partial y} \quad (4)$$

Near-wall eddy diffusivity D_t can be calculated by using the analogy between turbulent diffusion of momentum and mass, as in [32][19]:

$$D_t = \left(\frac{y^+}{C_t} \right)^3 \nu \quad (5)$$

where C_t is a constant that can range from 8.8 to 14.5 according to different authors [32,33], and y^+ is the dimensionless distance from the solid wall:

$$y^+ = \frac{y u^*}{\nu} \quad (6)$$

and the friction velocity is calculated as:

$$u^* = \sqrt{\tau/\rho} \quad (7)$$

Equation (5) is valid provided that the MT boundary layer is smaller than the viscous sublayer (i.e., for $\delta^+ < 5$) which is true for $Sc > 100$ typical for aqueous corrosion systems.

Finally, a mass balance for a given species can be written as:

$$\frac{\partial c}{\partial t} = \frac{\partial N}{\partial y} = \frac{\partial}{\partial y} \left((D + D_t) \frac{\partial c}{\partial y} \right) + R \quad (8)$$

where R is the chemical reaction source term. Solving the MT equation(s) above is no simple task, even with the mathematical simplification of the turbulent MT term. In multi-species MT with (electro)chemical reactions one deals with a set of transient, non-linear, coupled, partial differential equations (one equation (4) written for each species) with complex boundary conditions, which can be solved only by using numerical methods. Once this is done and species concentration profiles are resolved, the mass flux of a given species at the solid surface (wall) N_w , is obtained as:

$$N_w = D \frac{\partial c}{\partial y} \Big|_w \quad (9)$$

3. Mass transfer in gas-liquid pipe flow

3.1. Mass transfer coefficient calculation in gas-liquid flow via the Chilton-Colburn relationship

In order to determine the MT coefficient using the Chilton-Colburn analogy for the case of gas-liquid pipe flow, one needs to

¹ Here we are going to ignore electromigration that can be added to the analysis later, without any loss of generality.

estimate the values of mean velocity u and wall shear stress τ in [equation \(2\)](#) for the liquid phase (denoted as u_l and τ_l), given the liquid and gas flow rates and the pipe geometry (e.g., diameter and inclination). For this purpose, a multiphase gas-liquid flow model is needed, such as for example the one presented in the Appendix, in which the liquid flow characteristics can be calculated as a function of the gas-liquid flow pattern. Similar mechanistic gas-liquid flow models can be found elsewhere [34].

For the stratified, annular and dispersed bubble gas-liquid flow patterns, the liquid velocity u_l and wall shear stress τ_l in the liquid phase, obtained from a gas-liquid flow model, can then be directly used to obtain MT coefficients via [equation \(2\)](#). For the slug flow, the mean MT coefficient varies greatly with the passage of slugs and is computed as the weighted average of the MT coefficients for the liquid slug (k_{ms}) and the film (k_{mf}) portions:

$$k_m = k_{ms}\beta_s + k_{mf}(1 - \beta_s) = \left[\left(\frac{\tau_{ls}}{\rho_{ls}u_t^2} \right)^n u_t \beta_s + \left(\frac{|\tau_{lf}|}{\rho_l u_{lf}^2} \right)^n |u_{lf}| (1 - \beta_s) \right] Sc^{-2/3} \quad (10)$$

where u_t is the velocity of the liquid slug front, u_{lf} is the velocity of the liquid film, τ_{ls} and τ_{lf} are the wall shear stresses of the liquid slug and the liquid film, respectively; ρ_l is the density of the liquid, ρ_{ls} is the average density of the liquid slug ([equation \(A.26\)](#) in the Appendix), and β_s is the relative length of the liquid slug, as shown in [Fig. A1](#) and [equation \(A.23\)](#) in the Appendix. Note that the velocity $|u_{lf}|$ and the wall shear stress $|\tau_{lf}|$ of the liquid film are computed as absolute values, since they can be negative when the liquid film flows countercurrent in upward inclined and vertical slug flow.

3.2. Near-wall eddy diffusivity distribution calculation in gas-liquid flow

For stratified, annular and dispersed bubble gas-liquid flow patterns, the calculated wall shear stress in the liquid phase τ_l obtained from a gas-liquid flow model is needed for the calculation of the friction velocity u^* via [equation \(7\)](#). However, for slug flow, the situation is more complicated as the boundary layers in the liquid film and liquid slug are very different so an average friction velocity \bar{u}^* needs to be calculated by:

$$\bar{u}^* = u_{ls}^* \beta_s + u_{lf}^* (1 - \beta_s) = \sqrt{\frac{\tau_{ls}}{\rho_l}} \beta_s + \sqrt{\frac{|\tau_{lf}|}{\rho_l}} (1 - \beta_s) \quad (11)$$

where u_{ls}^* and u_{lf}^* are the friction velocities corresponding to the liquid slug and the liquid film. Then, \bar{u}^* is directly used in [equation \(6\)](#) to compute y^+ and the near-wall eddy diffusivity distribution expressed by [equation \(5\)](#) is fully defined.

It is worth mentioning that the modeling approaches presented above implicitly assume that the estimated MT rates are associated to the portion of pipe perimeter wetted by the water phase, which would not necessarily correspond to the entire pipe perimeter depending on various multiphase flow patterns. In dispersed bubble and bubble flow patterns the entire pipe circumference is wetted by liquid. In other circumstances where the liquid film is mostly occupying the bottom of the pipe (i.e., stratified flow), the liquid wetted perimeter is estimated as in [Fig. A1](#). (Appendix). In the case of horizontal or moderately inclined (e.g., $|\beta| < 45$ degrees) intermittent flows, the liquid film in the gas pocket wets mainly the bottom half of the pipe while the liquid slug cylinder does on the entire pipe circumference. Thus, [equations \(10\)](#) and [\(11\)](#) would represent the behavior of the bottom half of the pipe, which is believed to be the most unfavorable area of the pipe when it comes to corrosion since it is continuously wetted by liquid. On the other hand, if the pipe inclination is significant (i.e., $|\beta| > 45$ degrees) the existing flow pattern may be, e.g., slug or annular-mist which both

lead to an annular distribution of the liquid film (as part of the gas pocket area or continuous, respectively) and the liquid constantly wets the entire pipe circumference.

It can be noticed that the calculated MT rates will be directly related by the wall shear stresses exerted by the liquid phase which certainly depend on liquid and gas flow rates and flow pattern as described in the multiphase model provided in the Appendix. How these parameters and other parameters specific to the nature of multiphase flow (i.e., liquid holdup, relative slug length, etc.) can affect MT will not be discussed here since it exceeds the scope of this study and will be addressed in future publications.

Although the multiphase flow model in the appendix estimates a uniform wall shear stress and uniform MT rate for a given water-wet pipe perimeter, the proposed MT models can be applied to any multiphase flow calculations (including three-dimensional CFD simulations). These methods can give more realistic distributions of MT rates along the pipe perimeter but require significantly more computation resources, which may be impractical in many cases.

4. Results and discussion

4.1. Mass transfer in gas-water pipe flow

The models proposed above are compared with experimental data of ionic MT from Langsholt et al. [4] and Wang et al. [7] obtained in large-scale gas-water flows with stratified and slug flow patterns.

Langsholt et al. used an inclinable multiphase flow loop with an internal diameter 0.1 m and a length of 15 m. The gas phase was sulfur hexafluoride (SF_6) with reported density of 18.6 kg/m³ and calculated viscosity of 1.5×10^{-2} mPa·s at operating conditions (20°C and ~3 bar). The liquid phase was an aqueous solution 1 wt.% Na_2SO_4 with density of 1006 kg/m³ and viscosity of 1 mPa·s. MT rates were measured by the limiting current method using a platinum electrochemical probe, flush mounted at the bottom of the test section. Dissolved oxygen was the main reduced species with a $Sc = 473$. Liquid holdup was measured using gamma densitometry, which was calibrated by using the fast closing valves technique. The covered operating conditions and recorded flow patterns, as well as the measured average MT rates and liquid holdups are listed in [Table A1](#) in the Appendix.

Wang, et al. also used a multiphase flow loop with an internal diameter 0.1 m and a length of 15 m. The gas phase was nitrogen with estimated density of 1.15 kg/m³ and viscosity of 1.7×10^{-2} mPa·s at operating conditions (20°C and ~1.5bar). The liquid phase was an aqueous solution 0.01 M potassium ferri/ferrocyanide and 1 M NaOH for the MT measurements by the limiting current method. The calculated density and viscosities of the aqueous solution were 1043 kg/m³ and 1.1 mPa·s, respectively and the estimated $Sc = 1620$ [35]. The used operating conditions, observed flow patterns, and measured average MT rates are listed in [Table A2](#) in the Appendix.

It is worth mentioning that MT measurements obtained using the limiting current method have a linear dependence on the limiting current value and an inverse dependence on the bulk concentration of the used species. None of the authors of those studies provided specific information on the intrinsic error in their measurements, but it is reasonable to think that it might have been no more than 5% due to the use of advanced commercial potentiostats in both cases. Regarding the concentrations of the used species, none of the authors reported an uncertainty on the reported values. It can be assumed that the actual O_2 concentration in Langsholt et al.'s experiments might have had maximum fluctuations of about 5%; and the potassium ferrocyanide concentration in the solution used by Wang et al. might have had a maximum deviation of about 2%. Therefore, maximum uncertainties of about ± 10

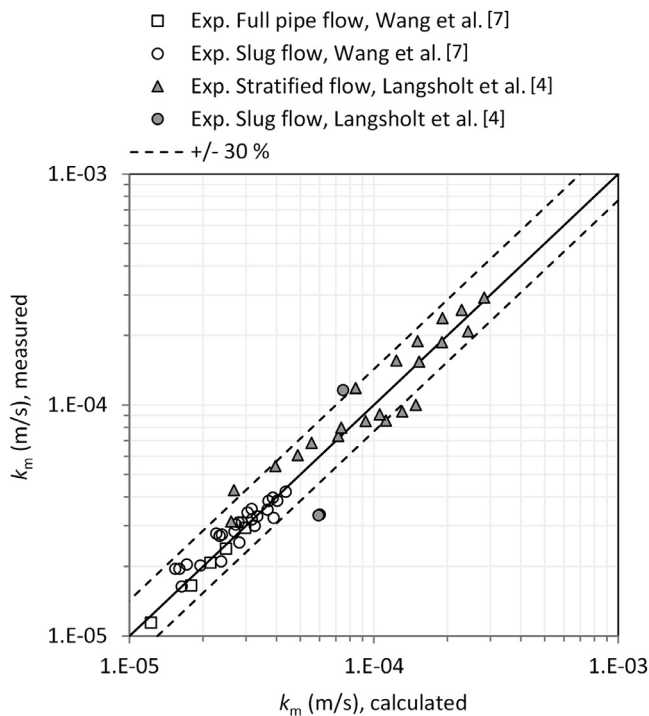


Fig. 3. Comparison between experimental mass transfer coefficients for large-scale gas-liquid pipe flow with different flow patterns and mass transfer coefficients calculated with Chilton-Colburn analogy equation (2) and equation (10).

% and $\pm 7\%$ may be expected on the data sets from Langsholt et al. and Wang, et al., respectively.

4.1.1. Calculated mass transfer coefficients in gas-liquid flow via the Chilton-Colburn relationship

Fig. 3 shows the comparison of the measured MT coefficients k_m in different conditions and flow patterns with the ones calculated via the Chilton-Colburn relationship, equation (2), based on the liquid phase velocity u_l and wall shear stress in the liquid phase τ_l calculated using the gas-liquid flow model presented in the Appendix. The agreement between the proposed model and the experimental data is good with a mean absolute error of 17% (equation A.41 in the Appendix), and of a total of 49 assessed data points, only 7 lie out of the $\pm 30\%$ error bounds. The cases with the largest discrepancy were the ones from 2° upward slug flow from Langsholt et al. [4]. A possible reason might be related to an overprediction of countercurrent flow liquid velocities in the liquid film by the simplified gas-liquid model presented in the Appendix.

MT predictions using the introduced mechanistic model are an improvement over correlations for gas-liquid flow found in the open literature, which are semi-empirical and mostly based on data from air-water flows in relatively small diameter pipes (e.g., 0.025m), as reviewed in the recent papers by Dong and Hibiki [36,37]. Most of these correlations are limited to horizontal or vertical flows, as well as relatively low superficial gas and liquid Reynolds numbers, making them unfeasible for large scale flows (e.g., large diameters and high gas and liquid flow rates) with different inclinations and upward and downward orientations. Among them, the correlation that performed slightly better when compared to the current experimental data with a mean absolute error of 20% is the one from Dong and Hibiki [37], which is based on vertical slug flow. However, it underestimates by about 70% the experimental MT rates measured in flows with liquid holdups smaller than 10%.

4.1.2. Calculated mass transfer coefficients in gas-liquid flow using the near-wall eddy diffusivity distribution

If we assume a steady state ($\partial c/\partial t = 0$) and no chemical reactions ($R = 0$), the partial differential equation (4) simplifies to an ordinary differential equation:

$$\frac{d}{dy} \left((D + D_t) \frac{dc}{dy} \right) = 0 \quad (12)$$

where D_t is a function of the distance from the wall, as shown by equations (5) – (7) above. This equation was solved numerically for all the experimental cases used in the comparisons below, by applying the finite difference method. The overall one-dimensional computational domain was set to be approximately four times the estimated diffusion boundary layer thickness ($\delta = D/k_m$). A species concentration equal to zero was imposed at the node representing the pipe surface and a unit concentration was set at the last node assumed to be in the bulk solution. A uniform computational mesh was employed. The number of used nodes was defined based on a mesh sensitivity analysis, where it was found that using at least 20 nodes over the length of the diffusion boundary layer (more than 80 nodes in the entire wall distance domain) showed a deviation of less than -2% on the calculated wall flux respect to the use of 40 or more nodes. Consequently, all the numerical calculations shown here were performed using at least 20 nodes to resolve the concentration profile in the diffusion boundary layer.

Turbulent diffusivity was calculated by using equation (5) with $C_t = 8.85$ as suggested by Davies [33] but also with $C_t = 14.5$ as suggested by Lin et al. [32]. Furthermore, the eddy diffusivity functions suggested by Notter and Sleicher [38] and Aravinth [39] were also evaluated:

$$D_t = \frac{C_1 y^{+3}}{(1 + C_2 y^{+2})^{1/2}} \nu_l \quad (13)$$

where ν_l is the kinematic viscosity of the liquid, and C_1 and C_2 are constants of value 9×10^{-4} and 6.7×10^{-3} for Notter and Sleicher and 7×10^{-4} and 4.05×10^{-3} for Aravinth, respectively.

The calculated results are presented below in terms of an effective MT coefficient, which can be calculated from the known concentration profile and the wall flux equation (4), as:

$$k_m = \frac{N_w}{(c_w - c_b)} \quad (14)$$

where c_b and c_w are the concentrations of a given species in the bulk of the fluid and at the wall, respectively.

As an illustration of how these different eddy diffusivity functions perform in single-phase flow, they were first compared with the established MT correlation for turbulent straight pipe of Berger and Hau, as shown in Fig. 4. These calculations were performed using $Sc = 200$, which corresponds to water properties at 20°C and a generic species with diffusion coefficient of $5 \times 10^{-9} \text{ m}^2/\text{s}$. The eddy diffusivity approach in all cases reproduces the same slope of k_m vs. Re number as the Berger and Hau correlation, however, the eddy diffusivity expressions suggested by Davies, Notter and Sleicher, and Aravinth overestimate the MT rates by an average of more than 50%. The Lin et al. expression gives somewhat better results with an average overestimation of 21%. Similar results were found for calculations performed using $Sc = 1000$.

Therefore, the Lin et al. expression was then used to calculate the MT coefficients for gas-liquid flow and compared with the experimental values in Fig. 5. Calculations show a significant overestimation of MT rates with a mean absolute error of 34%. Moreover, about 50% of the data are out of the 30% error band, including the single-phase flow data of Wang, et al. (42% average error). This was expected since Lin et al. expression overestimates MT rates in single phase flow calculated by the Berger and Hau correlation by

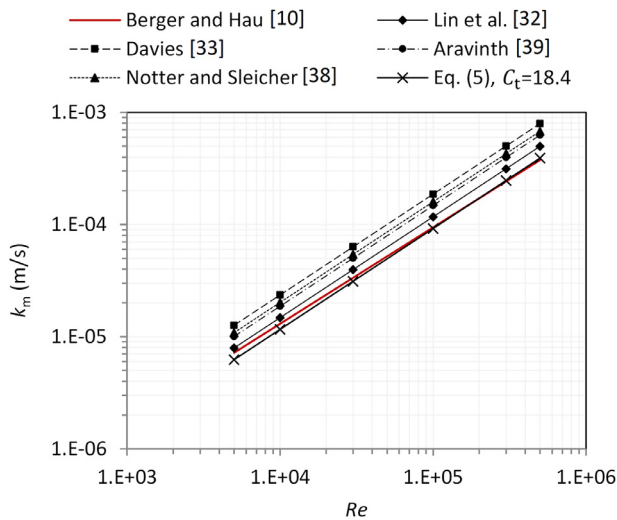


Fig. 4. Comparison between mass coefficients for single phase pipe flow calculated with the eddy diffusivity approach, equations (5) and (13), and Berger and Hau's correlation. $Sc = 200$, $d = 0.1$ m, $\rho_l = 1000$ kg/m³, $\mu_l = 1$ mPa.s.

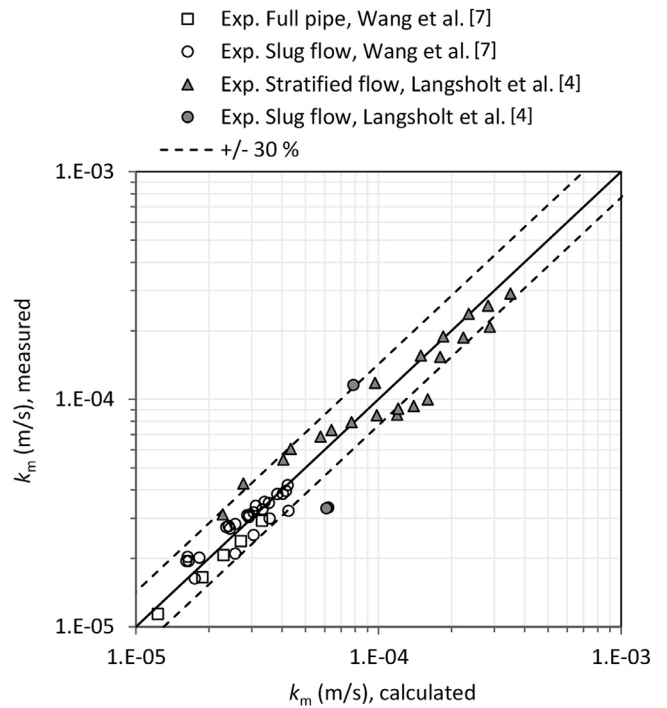


Fig. 6. Comparison between experimental mass transfer coefficients for large-scale gas-liquid pipe flow with different flow patterns and mass transfer coefficients calculated with the eddy diffusivity approach, equation (5) with $C_t = 18.4$.

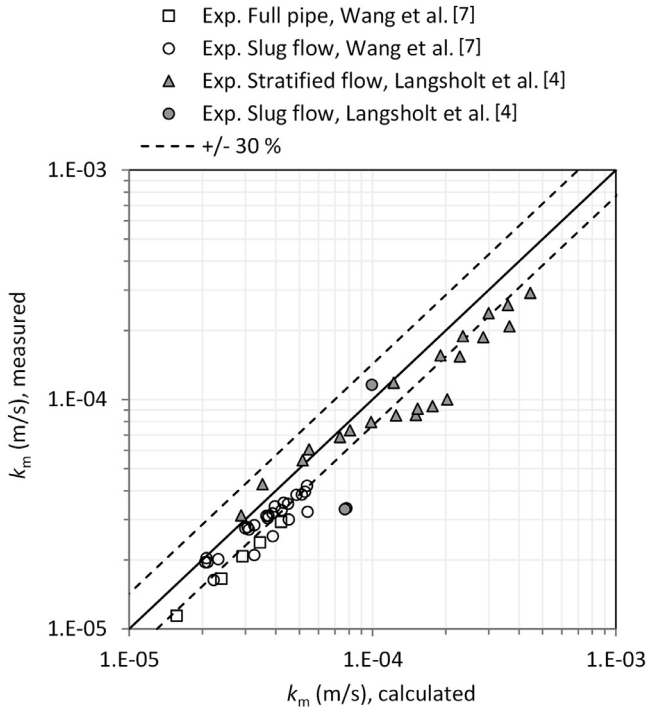


Fig. 5. Comparison between experimental mass transfer coefficients for large-scale gas-liquid pipe flow with different flow patterns and mass transfer coefficients calculated with the eddy diffusivity approach, equation (5) using Lin et al.'s formulation [32].

more than 20% on average, as shown in Fig. 4. When we adjusted the coefficient C_t in equation (5) to a value of 18.4, this led to a decrease on the mean absolute error in single-phase flow to about 6% with respect to Berger and Hau's correlation (Fig. 4), and a decrease of the mean absolute error to 19% with respect to the experimental data from gas-liquid flow, as shown in Fig. 6. Even higher values of C_t do not improve the mean absolute error of prediction in gas-liquid flow significantly, and lead to a more serious underestimation of MT in single-phase flow, by more than 10% on average.

4.2. Mass transfer in gas-oil-water and oil-water pipe flow

In the case of gas-oil-water flows, the produced oil and water phases can flow either separated or mixed. If flow conditions (e.g., gas, oil and water flow rates) are high enough to produce the full entrainment of the water in the oil phase, the pipe wall will not likely be water wet and MT of corrosive species will be suppressed [40,41]. However, if water either segregates from the mix or becomes the continuous phase, MT rates are similar to the ones seen corresponding to gas-water flow (without oil) [8]. Therefore, calculation of MT rates in gas-oil-water flow can still be done using the Chilton-Colburn analogy, equation (2) or the eddy diffusivity approach, equation (5) by using liquid velocities and wall shear stresses calculated with a multiphase flow model and the following liquid mixture properties:

$$\rho_{lm} = \rho_o(1 - \varepsilon_w) + \rho_w \varepsilon_w \quad (15)$$

$$\mu_{lm} \cong \begin{cases} \mu_o & \varepsilon_w < IP \\ \mu_w & \varepsilon_w > IP \end{cases} \quad (16)$$

where ρ_{lm} and μ_{lm} are the density and the viscosity of the liquid mixture, respectively; ρ_o and μ_o are the density and viscosity of the oil phase, ρ_w and μ_w are the density and viscosity of the water phase, IP is the phase inversion point of the oil-water mixture based on the water volume content (for crude oil can be approximated as 0.5); and ε_w is the volumetric water fraction in the liquid mix, which can be approximated as the water cut (assuming no slip between oil and water phases):

$$\varepsilon_w = \frac{u_{sw}}{u_{sw} + u_{so}} = \frac{u_{sw}}{u_{sl}} \quad (17)$$

where u_{so} and u_{sw} are the superficial velocities of oil and water respectively; their sum is the total superficial liquid velocity u_{sl} . Sc number is obviously calculated using the physical properties of the water phase.

In the case of oil-water flow (with negligible or no gas phase present), the calculation of MT rates is performed similarly as to gas-liquid flow. However, a different oil-water flow model is required for the estimation of the velocity and wall shear stress of the water phase, which will be presented in the following publications.

5. Summary and conclusions

Two different approaches for mass transfer calculation in multiphase gas-liquid flow have been introduced and compared against experimental data from large-scale flows with different flow patterns. In general, the agreement of the presented mass transfer models with the available experimental data is reasonably good for all the different flow patterns; this was particularly difficult to achieve in slug flow where the hydrodynamic and diffusion boundary layers fluctuate over relatively short time scales.

Computation of integral mass transfer coefficients can be done with reasonable accuracy for a wide variety of flows (single phase pipe and rotating cylinder, and two-phase gas-liquid pipe) by using the fundamental Chilton-Colburn analogy with an exponent of 0.96 on the friction factor.

Mass transfer rate calculations using the eddy diffusivity approach tend to overestimate the measured mass transfer rates in single and multiphase flow when some of the well-known formulations from the literature are used. However, when the standard eddy diffusivity function with a cubic dependence on the dimensionless wall distance, is coupled with a coefficient of 18.4, this proved to be the most appropriate way to predict mass transfer rates in single and multiphase flow, which performed much better than the other proposed functions in the open literature.

The main strength of the proposed models is their mechanistic nature, which allows their use in systems with wide range of physical properties (different gas and liquid densities and viscosities), pipe characteristics (different diameters, inclinations, both smooth and rough surfaces), and fluids flow rates. Moreover, better results can be achieved if liquid flow characteristics are estimated using multiphase flow models that are more advanced and refined than the one currently presented. Overall, the present approach is a significant improvement over semi-empirical correlations found in the literature that are usually appropriate for limited ranges of fluid's properties and flow rates, making them unreliable for general use. In addition, these semi-empirical correlations cannot be used in more complicated mass transfer scenarios, where (electro)chemical reactions and/or ionic species are involved, while the present approach can, with satisfactory results.

Declaration of Competing Interest

The authors declare that they have no known competing financial interests or personal relationships that could have appeared to influence the work reported in this paper.

Appendix

A.1. Experimental data used in the model validation

See [Table A1](#) and [Table A2](#).

A.2. Turbulent single-phase pipe flow

Friction factor, Blasius equation:

$$f = 0.046Re^{-0.2} \quad Re > 2100 \quad (A.1)$$

Mass transfer correlation, Berger and Hau [10]:

$$Sh = 0.0165Re^{0.86}Sc^{0.33}; \quad 8 \times 10^3 \leq Re \leq 2 \times 10^5; \quad 10^3 \leq Sc \leq 6 \times 10^3 \quad (A.2)$$

Table A1

Experimental conditions, measured liquid holdup and average mass transfer rates in horizontal and slightly inclined flow from Langsholt et al. [4].

Flow pattern	u_{sl} (m/s)	u_{sg} (m/s)	β (°)	α_l (%)	Sh
Strat.-wavy	0.021	2.14	0	6.1	1,489
Strat.-wavy	0.019	4.11	0	2	2,884
Strat.-wavy	0.025	6.34	0	1.2	3,491
Strat.-wavy	0.25	6.06	0	11.1	4,076
Strat.-wavy	0.25	7.1	0	9.5	4,450
Strat.-wavy	0.25	8.18	0	8.2	4,762
Strat.-wavy	0.25	5.05	0	12.9	4,053
Strat.-wavy	0.25	4.1	0	15.4	3,788
Strat.-wavy	0.25	3	0	19.4	3,265
Strat.-wavy	0.25	2.03	0	27.2	2,587
Strat.-wavy	0.25	0.96	0	42	2,034
Strat.-wavy	2	3	2	50	7,404
Strat.-wavy	2	5	2	31	8,986
Strat.-wavy	2	7	2	21	11,300
Strat.-wavy	2	9	2	17	12,275
Strat.-wavy	2	12	2	13	13,888
Strat.-wavy	1	3	2	42	5,627
Strat.-wavy	1	7	2	19	7,326
Strat.-wavy	1	9	2	14	8,892
Strat.-wavy	1	12	2	9	9,913
Strat.-wavy	0.78	5	2	43	4,333
Slug	0.78	2	2	30	5,518
Slug	0.13	2	2	26	1,598
Slug	0.1	2	2	25	1,582

Table A2

Experimental conditions and measured average mass transfer rates in horizontal flow from Wang et al. [7].

Flow pattern	u_{sl} (m/s)	u_{sg} (m/s)	Sh
Full liquid	0.5	0	1,756
Full liquid	0.8	0	2,543
Full liquid	1	0	3,189
Full liquid	1.2	0	3,669
Full liquid	1.5	0	4,509
Slug	0.5	0.6	2,514
Slug	0.8	0.6	3,232
Slug	1	0.6	3,903
Slug	1.2	0.6	4,613
Slug	1.5	0.6	4,986
Slug	0.5	1.4	3,001
Slug	0.8	1.4	4,272
Slug	1	1.4	4,672
Slug	1.2	1.4	5,451
Slug	1.5	1.4	6,101
Slug	0.5	2.4	3,001
Slug	0.8	2.4	4,168
Slug	1	2.4	4,777
Slug	1.2	2.4	5,255
Slug	1.5	2.4	5,904
Slug	0.5	3.6	3,131
Slug	0.8	3.6	4,227
Slug	1	3.6	4,777
Slug	1.2	3.6	5,060
Slug	1.5	3.6	5,919
Slug	0.5	4.8	3,102
Slug	0.8	4.8	4,361
Slug	1	4.8	4,911
Slug	1.2	4.8	5,406
Slug	1.5	4.8	6,466

A.3. Turbulent single-phase rotating cylinder flow

Friction factor [15]:

$$\frac{f}{2} = 0.079Re_{cyl}^{-0.3}; \quad 1000 \leq Re_{cyl} \leq 100,000 \quad (A.3)$$

$$Re_{cyl} = \frac{2\rho r_{cyl}u_{cyl}}{\mu}; \quad (A.4)$$

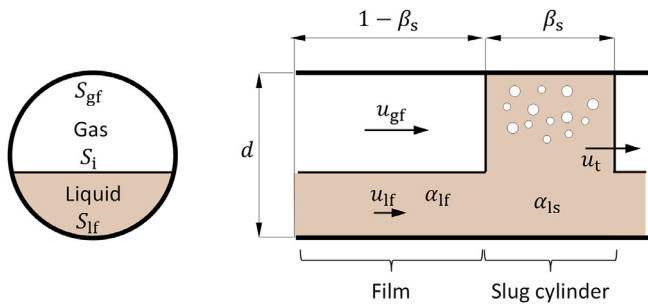


Fig. A1. Schematic representation of the slug flow unit assumed in the gas-liquid model.

$$u_{\text{cyl}} = \omega r_{\text{cyl}} \quad (\text{A.5})$$

where r_{cyl} is the radius of the rotating cylinder, and ω is the rotational speed of the cylinder.

Mass transfer correlation [15]:

$$Sh_{\text{cyl}} = 0.079 Re_{\text{cyl}}^{0.7} Sc^{0.356}; \quad 1000 \leq Re_{\text{cyl}} \leq 100,000 \quad (\text{A.6})$$

$$Sh_{\text{cyl}} = \frac{2k_m r_{\text{cyl}}}{D} \quad (\text{A.7})$$

A.4. Gas-liquid flow model

A.4.1. Flow pattern map determination

The boundary for stratified/non-stratified flow (line 1 in Fig. 1) can be estimated using the approach of Kelvin-Helmholtz instability of interfacial waves suggested by Taitel and Dukler [42]. The boundary slug/annular flow (line 2 in Fig. 1) can be computed using the criterion suggested by Barnea [1] of liquid holdup (α_l) larger or equal to 0.24 for intermittent flow. The boundary dispersed bubble/slug flow (line 3 in Fig. 1) can be calculated using the criterion $d_{\text{max}} \leq d_{\text{crit}}$ suggested by Brauner [43], where d_{max} is the maximum bubble size in the flow and d_{crit} is a critical bubble size based on the balance of turbulent and buoyant forces and excessive deformation of dispersed bubbles. Line 4 in Fig. 1 is computed from the maximum gas holdup that can be entrained in the liquid phase ($\alpha_{g\text{max}} = 0.52$) as suggested by Taitel et al. [44]. A region of "bubble" flow pattern, between dispersed bubble and intermittent flow, can also exist in inclined and vertical pipes [44,45]. The boundary bubble/slug flow can be determined by a critical gas holdup or void fraction ($\alpha_{g\text{crit}} = 0.25$) as suggested in [45]; thus, bubble flow occurs if $\alpha_g < \alpha_{g\text{crit}}$, and intermittent flow happens when $\alpha_g \geq \alpha_{g\text{crit}}$.

A.4.2. Slug flow characteristics

The gas pocket/liquid film region of the slug unit can be modeled by using the combined momentum balance at steady state for stratified liquid and gas in a pipe based on the simplified geometry shown in Fig. A1:

$$\frac{\tau_{\text{gf}} S_{\text{gf}}}{\alpha_{\text{gf}}} - \frac{\tau_{\text{lf}} S_{\text{lf}}}{\alpha_{\text{lf}}} + \tau_i S_i \left(\frac{1}{\alpha_{\text{lf}}} + \frac{1}{\alpha_{\text{gf}}} \right) - A(\rho_l - \rho_g) g \sin \beta = 0 \quad (\text{A.8})$$

where τ_{gf} , τ_{lf} and τ_i are the wall shear stresses due to the flow of the gas bubble and the liquid film, respectively; τ_i is the shear stress at the gas-liquid interface, α_{gf} (also expressed as: $1 - \alpha_{\text{lf}}$) and α_{lf} are the fractions of pipe cross-sectional area (A) occupied by gas and liquid, respectively; S_{gf} and S_{lf} are the pipe perimeters wetted by gas and liquid, respectively; S_i is the perimeter of the gas-liquid interface, ρ_g is the gas density; g is the gravitational acceleration, and β is the pipe inclination angle measured from the horizontal. The wall shear stresses are calculated as follows:

$$\tau_{\text{gf}} = \frac{1}{2} f_{\text{gf}} \rho_g u_{\text{gf}}^2 \quad (\text{A.9})$$

$$\tau_{\text{lf}} = \frac{1}{2} f_{\text{lf}} \rho_l u_{\text{lf}}^2 \quad (\text{A.10})$$

and the interfacial shear stress:

$$\tau_i = \frac{1}{2} f_i \rho_g (u_{\text{gf}} - u_{\text{lf}}) |u_{\text{gf}} - u_{\text{lf}}| \quad (\text{A.11})$$

where u_{gf} and u_{lf} are the mean velocities of the gas and liquid; respectively; and f_{gf} , f_{lf} and f_i are the friction factors for the gas bubble, liquid film and gas-liquid interface, respectively. Friction factors are estimated as:

$$f = C_f Re^{-n_f} \quad (\text{A.12})$$

where Re is the Reynolds number, and C_f and n_f are constants equal to 0.046 and 0.2, respectively; for turbulent flow $Re > 2100$, and 16 and 1 for laminar flow $Re \leq 2100$. In case the pipe surface is not hydraulically smooth, the explicit friction factor formulas in [46] can be used. The Reynolds numbers for the gas bubble and liquid film flows are:

$$Re_g = \frac{\rho_g u_{\text{gf}} d_{\text{gf}}}{\mu_g} \quad (\text{A.13})$$

$$Re_{\text{lf}} = \frac{\rho_l u_{\text{lf}} d_{\text{lf}}}{\mu_l} \quad (\text{A.14})$$

and gas-liquid interface:

$$Re_i = \frac{\rho_g |u_{\text{gf}} - u_{\text{lf}}| d_{\text{gf}}}{\mu_g} \quad (\text{A.15})$$

where μ_g and μ_l are the viscosities of the gas and the liquid, respectively; d_{gf} is the hydraulic diameter for the gas bubble flow:

$$d_{\text{gf}} = \frac{4A\alpha_{\text{gf}}}{S_{\text{lg}} + S_i} \quad (\text{A.16})$$

and d_{lf} is the hydraulic diameter of the liquid film flow:

$$d_{\text{lf}} = \frac{4A\alpha_{\text{lf}}}{S_{\text{lf}}} \quad (\text{A.17})$$

The mean velocity of the liquid slug cylinder is approximated to the mixture velocity, which is calculated as the summation of superficial gas and liquid velocities:

$$u_m = u_{\text{sg}} + u_{\text{sl}} \quad (\text{A.18})$$

No slip is considered between the entrained gas bubbles and the liquid in the slug cylinder. Then, the velocities of the gas bubble and the liquid film can be related with the gas bubble and liquid film holdups (α_{gf} and α_{lf} , respectively) as suggested by Dukler and Hubbard [47]:

$$u_{\text{gf}} = u_t + (u_m - u_t) \left(\frac{1 - \alpha_{\text{ls}}}{1 - \alpha_{\text{lf}}} \right) \quad (\text{A.19})$$

$$u_{\text{lf}} = u_t \left(1 - \frac{\alpha_{\text{ls}}}{\alpha_{\text{lf}}} \right) + u_m \frac{\alpha_{\text{ls}}}{\alpha_{\text{lf}}} \quad (\text{A.20})$$

where α_{ls} is the liquid holdup at the slug cylinder, and u_t is the translational velocity at which the slug propagates, and is estimated as:

$$u_t = C_0 u_m + u_b \quad (\text{A.21})$$

where u_b (m/s) is the Taylor bubble velocity that can be neglected in horizontal slug flow, C_0 is the distribution parameter used in the drift-flux model and can be approximated with the value 1.2 [48].

The liquid holdup at the slug cylinder is approximated using the Gregory et al. correlation [49]:

$$\alpha_{ls} = \left[1 + \left(\frac{u_m}{8.66} \right)^{1.39} \right]^{-1} \quad (\text{A.22})$$

The constant 8.66 in equation above has SI velocity units.

The combined momentum balance in equation (A.8) can be solved iteratively to find the liquid film holdup (α_{lf}). Since equation (A.8) has multiple roots for pipe inclination angles (β) different than zero; in general, the smaller root is considered as solution of the problem.

From the conservation of the liquid mass in the slug unit (liquid film + slug cylinder), the relative length of the slug cylinder is estimated in terms of the superficial liquid velocity and the velocities and the liquid holdups of the film and the slug cylinder:

$$\beta_s = \frac{u_{sl} - u_{lf} \alpha_{lf}}{u_m \alpha_{ls} - u_{lf} \alpha_{lf}} \quad (\text{A.23})$$

Then, the average liquid holdup in the slug unit is:

$$\alpha_1 = \alpha_{ls} \beta_s + \alpha_{lf} (1 - \beta_s) \quad (\text{A.24})$$

The shear stress at the liquid slug is estimated as:

$$\tau_{ls} = \frac{1}{2} f_{ls} \rho_{ls} u_t^2 \quad (\text{A.25})$$

The friction factor f_{ls} is calculated as in (A.12) but using the Reynolds number $\rho_{ls} u_t d / \mu_{ls}$, where the density and viscosity of the liquid slug are:

$$\rho_{ls} = \rho_l \alpha_{ls} + \rho_g (1 - \alpha_{ls}) \quad (\text{A.26})$$

$$\mu_{ls} = \mu_l \alpha_{ls} + \mu_g (1 - \alpha_{ls}) \quad (\text{A.27})$$

A.4.3. Stratified and annular-mist flow characteristics

The combined momentum equation (A.8) is also used to calculate flow characteristics in stratified and annular-mist flow. In the case of the latter, the liquid is assumed to occupy mostly the pipe bottom (as shown in Fig. A1) for inclination angles of absolute value smaller than 45 degrees. For relatively high gas velocities, a fraction of the liquid can be entrained by the gas flow, which can be calculated as [50]:

$$E = \left\{ 1 - \exp \left[-0.125 \left(10^4 \frac{u_{sg} \mu_g}{\sigma} \sqrt{\frac{\rho_g}{\rho_l}} - 1.5 \right) \right] \right\} \quad (\text{A.28})$$

Then, the liquid holdup is:

$$\alpha_1 = \alpha_{lf} + \frac{u_{sl} E}{(u_{sg} + u_{sl} E)} \quad (\text{A.29})$$

Note that if $E = 0$ then $\alpha_1 = \alpha_{ls}$. If $E > 0$, the gas holdup (α_{gf}) in equation (A.8) is now the holdup of a combined gas-liquid flow. The velocity of the liquid film is:

$$u_{lf} = \frac{u_{sl} (1 - E)}{\alpha_{lf}} \quad (\text{A.30})$$

The velocity of the gas or gas-liquid mix ($E > 0$, no slip between the entrained liquid drops and the gas) is:

$$u_{gf} = \frac{(u_{sg} + u_{sl} E)}{\alpha_{gf}} \quad (\text{A.31})$$

When solving equation (A.8) a different interfacial friction closure relationship is used instead of equation (A.11):

$$\tau_i = \frac{1}{2} f_i \rho_{gf} (u_{gf} - u_i) |u_{gf} - u_i| \quad (\text{A.32})$$

where u_i is the velocity of the interface between the liquid film and the gas calculated as in Oliemans et al. [51]. The interfacial

friction factor (f_i) is calculated with the Colebrook equation using an effective roughness described in [51], the hydraulic diameter (d_{gf}) and the Reynolds number $\rho_{gf} u_{gf} d_{gf} / \mu_{gf}$, where:

$$\rho_{gf} = \rho_l (1 - \alpha_{gr}) + \rho_g \alpha_{gr} \quad (\text{A.33})$$

$$\mu_{gf} = \mu_l (1 - \alpha_{gr}) + \mu_g \alpha_{gr} \quad (\text{A.34})$$

$$\alpha_{gr} = \frac{u_{sg}}{(u_{sg} + u_{sl} E)} \quad (\text{A.35})$$

Note that the density and viscosity calculated with equations (A.33) and (A.34) replace the gas density and viscosity in equations (A.9) and (A.13).

A.4.4. Dispersed bubble and bubble flow characteristics

A homogeneous no-slip model is used to estimate flow characteristics in dispersed bubble flow. Therefore, the velocity of the liquid and the entrained gas bubbles is considered to be similar to the mixture velocity:

$$u_1 = u_g \cong u_m \quad (\text{A.36})$$

The liquid holdup is:

$$\alpha_1 = \frac{u_{sl}}{(u_{sg} + u_{sl})} \quad (\text{A.37})$$

The wall shear stress is:

$$\tau_1 = \frac{1}{2} f_m \rho_m u_1^2 \quad (\text{A.38})$$

where the friction factor f_m is calculated as in (A.12) using the Reynolds number $\rho_m u_1 d / \mu_m$, where:

$$\rho_m = \rho_l \alpha_1 + \rho_g (1 - \alpha_1) \quad (\text{A.39})$$

$$\mu_m = \mu_l \alpha_1 + \mu_g (1 - \alpha_1) \quad (\text{A.40})$$

Bubble flow can have significant slip between the liquid and the gas bubbles which rise quicker due to buoyancy. In this case, a drift flux model can be used to properly determine the liquid and gas holdups. Equations (A.38 to A.40) can then be used to calculate flow characteristics.

A.5. Definition of errors

Mean absolute error (%):

$$\bar{e} = \frac{\sum_{i=1}^m \frac{|x_i - z_i|}{z_i}}{m} 100 \quad (\text{A.41})$$

where x_i is the value of the calculated parameter, z_i is the value of the parameter measured experimentally, and m is the number of evaluated points.

CRediT authorship contribution statement

Luciano D. Paolinelli: Conceptualization, Investigation, Methodology, Writing - review & editing, Data curation, Visualization, Formal analysis, Software. **Srdjan Nesic:** Conceptualization, Investigation, Methodology, Writing - review & editing.

References

- [1] D. Barnea, A unified model for predicting flow-pattern transitions for the whole range of pipe inclinations, *Int. J. Multiph. Flow.* 13 (1987) 1–12.
- [2] S. Nešić, A. Kahyarian, Y.S. Choi, Implementation of a Comprehensive Mechanistic Prediction Model of Mild Steel Corrosion in Multiphase Oil and Gas Pipelines, *Corrosion* 75 (2019) 274–291.
- [3] Y. Zheng, J. Ning, B. Brown, S. Nešić, Advancement in Predictive Modeling of Mild Steel Corrosion in CO₂- and H₂S-Containing Environments, *Corrosion* 72 (2016) 679–691.

- [4] M. Langsholt, M. Nordsveen, K. Lunde, S. Nescic, J. Enerhaug, in: *Wall Shear Stress and Mass Transfer Rates – Important Parameters in CO₂ Corrosion*, BHR Gr. Multiph. '97, BHR Group, Cannes, France, 1997, pp. 537–552.
- [5] N. Pecherkin, V.C.E.-M. El-Amin (Ed.), *IntechOpen*, Rijeka, 2011 Ch. 8.
- [6] H. Wang, H.D. Dewald, W.P. Jepson, Mass-Transfer Enhancement in Large-Diameter Pipeline under Water/Gas Stationary Slug Flow, *J. Electrochem. Soc.* 151 (2004) B114–B123.
- [7] H. Wang, T. Hong, J.-Y. Cai, W.P. Jepson, Enhanced Mass Transfer and Wall Shear Stress in Multiphase Slug Flow, *NACE Corrosion 2002*, NACE, Houston TX, 2000, Paper 2501.
- [8] H. Wang, D. Vedapuri, J.Y. Cai, T. Hong, W.P. Jepson, Mass Transfer Coefficient Measurement in Water/Oil/Gas Multiphase Flow, *J. Energy Resour. Technol.* 123 (2000) 144–149.
- [9] K. Yan, Y. Zhang, D. Che, Experimental study on near wall transport characteristics of slug flow in a vertical pipe, *Heat Mass Transf.* 48 (2012) 1193–1205.
- [10] F.P. Berger, K.F.L. Hau, Mass transfer in turbulent pipe flow measured by the electrochemical method, *Int. J. Heat Mass Transf.* 20 (1977) 1185–1194.
- [11] S. Wang, S. Nescic, On Coupling CO₂ Corrosion and Multiphase Flow Models, *NACE Corrosion 2003*, NACE, Houston TX, Paper 3631.
- [12] T.H. Chilton, A.P. Colburn, Mass Transfer (Absorption) Coefficients Prediction from Data on Heat Transfer and Fluid Friction, *Ind. Eng. Chem.* 26 (1934) 1183–1187.
- [13] S.W. Churchill, Comprehensive Correlating Equations for Heat, Mass and Momentum Transfer in Fully Developed Flow in Smooth Tubes, *Ind. Eng. Chem. Fundam.* 16 (1977) 109–116.
- [14] D.W. Hubbard, E.N. Lightfoot, Correlation of Heat and Mass Transfer Data for High Schmidt and Reynolds Numbers, *Ind. Eng. Chem. Fundam.* 5 (1966) 370–379.
- [15] M. Eisenberg, C.W. Tobias, C.R. Wilke, Ionic Mass Transfer and Concentration Polarization at Rotating Electrodes, *J. Electrochem. Soc.* 101 (1954) 306–320.
- [16] S. Nešić, J. Postlethwaite, D.J. Bergstrom, Calculation of wall-mass transfer rates in separated aqueous flow using a low Reynolds number κ - ϵ model, *Int. J. Heat Mass Transf.* 35 (1992) 1977–1985.
- [17] S. Nešić, G. Adamopoulos, J. Postlethwaite, D.J. Bergstrom, Modelling of turbulent flow and mass transfer with wall function and low-reynolds number closures, *Can. J. Chem. Eng.* 71 (1993) 28–34.
- [18] C. Rosén, C. Trägårdh, Prediction of turbulent high Schmidt number mass transfer using a low Reynolds number k - ϵ turbulence model, *Chem. Eng. J. Biochem. Eng. J.* 59 (1995) 153–159.
- [19] Y. Wang, J. Postlethwaite, D.J. Bergstrom, Modelling mass transfer entrance lengths in turbulent pipe-flow with applications to small cathodes for measuring local mass transfer rates, *J. Appl. Electrochem.* 26 (1996) 471–479.
- [20] Y. Wang, J. Postlethwaite, The application of low Reynolds number k - ϵ turbulence model to corrosion modelling in the mass transfer entrance region, *Corros. Sci.* 39 (1997) 1265–1283.
- [21] E. Duran, F. Taghipour, M. Mohseni, CFD modeling of mass transfer in annular reactors, *Int. J. Heat Mass Transf.* 52 (2009) 5390–5401.
- [22] J. Xiong, S. Koshizuka, M. Sakai, Turbulence modeling for mass transfer enhancement by separation and reattachment with two-equation eddy-viscosity models, *Nucl. Eng. Des.* 241 (2011) 3190–3200.
- [23] M. van Reeuwijk, M. Hadžiabdić, Modelling high Schmidt number turbulent mass transfer, *Int. J. Heat Fluid Flow* 51 (2015) 42–49.
- [24] A. Kahyarian, S. Nescic, A New Narrative for CO₂ Corrosion of Mild Steel, *J. Electrochem. Soc.* 166 (2019) C3048–C3063.
- [25] A. Kahyarian, S. Nescic, H₂S corrosion of mild steel: A quantitative analysis of the mechanism of the cathodic reaction, *Electrochim. Acta.* 297 (2019) 676–684.
- [26] X. Li, H. Hu, G. Cheng, Y. Li, W. Wu, Y. Xia, W. Wu, Numerical Predictions of Mild-Steel Corrosion in a H₂S Aqueous Environment Without Protective Product Layers, *Corrosion* 73 (2017) 786–795.
- [27] O. Dolgikh, A.C. Bastos, A. Oliveira, C. Dan, J. Deconinck, Influence of the electrolyte film thickness and NaCl concentration on the oxygen reduction current on platinum, *Corros. Sci.* 102 (2016) 338–347.
- [28] H.-Q. Zhang, Q. Wang, C. Sarica, J.P. Brill, A unified mechanistic model for slug liquid holdup and transition between slug and dispersed bubble flows, *Int. J. Multiph. Flow.* 29 (2003) 97–107.
- [29] H.-Q. Zhang, C. Sarica, Unified Modeling of Gas/Oil/Water Pipe Flow - Basic Approaches and Preliminary Validation, *SPE Proj. Facil. Constr.* 1 (2006) 1–7.
- [30] J.S. Newman, *Electrochemical Systems*, Prentice-Hall, 1972.
- [31] M.H. Mamme, J. Deconinck, J. Ustarroz, Transition between kinetic and diffusion control during the initial stages of electrochemical growth using numerical modelling, *Electrochim. Acta.* 258 (2017) 662–668.
- [32] C.S. Lin, R.W. Moulton, G.L. Putnam, Mass Transfer between Solid Wall and Fluid Streams. Mechanism and Eddy Distribution Relationships in Turbulent Flow, *Ind. Eng. Chem.* 45 (1953) 636–640.
- [33] J.T. Davies, Eddy Transfer Near Solid Surfaces, in: *Turbul. Phenom.*, Elsevier, Netherlands, 1972, pp. 121–174.
- [34] O. Shoham, Mechanistic modeling of gas-liquid two-phase flow in pipes, *Society of Petroleum Engineers/AIME*, Richardson TX, 2006.
- [35] S.L. Gordon, J.S. Newman, C.W. Tobias, The role of ionic migration in electrolytic mass transport; Diffusivities of [Fe(CN)₆]³⁻ and [Fe(CN)₆]⁴⁻ in KOH and NaOH solutions, *Berichte Der Bunsengesellschaft Für Phys. Chemie.* 70 (1966) 414–420.
- [36] C. Dong, T. Hibiki, Heat transfer correlation for two-component two-phase slug flow in horizontal pipes, *Appl. Therm. Eng.* 141 (2018) 866–876.
- [37] C. Dong, T. Hibiki, Correlation of heat transfer coefficient for two-component two-phase slug flow in a vertical pipe, *Int. J. Multiph. Flow.* 108 (2018) 124–139.
- [38] R.H. Nottter, C.A. Sleicher, The eddy diffusivity in the turbulent boundary layer near a wall, *Chem. Eng. Sci.* 26 (1971) 161–171.
- [39] S. Aravindh, Prediction of heat and mass transfer for fully developed turbulent fluid flow through tubes, *Int. J. Heat Mass Transf.* 43 (2000) 1399–1408.
- [40] K.E. Kee, M. Babic, S. Richter, L. Paolinelli, W. Li, S. Nescic, Flow patterns and water wetting in gas-oil-water three-phase flow - A flow loop study, *NACE Corrosion 2015*, NACE, Houston TX, 2015, Paper 6113.
- [41] L.D. Paolinelli, Study of Phase Wetting in Three-Phase Oil-Water-Gas Horizontal Pipe Flow - Recommendations for Corrosion Risk Assessment, *NACE Corrosion 2018*, NACE, Houston TX, 2018, Paper 11213.
- [42] Y. Taitel, A.E. Dukler, A model for predicting flow regime transitions in horizontal and near horizontal gas-liquid flow, *AIChE J* 22 (1976) 47–55.
- [43] N. Brauner, The prediction of dispersed flows boundaries in liquid-liquid and gas-liquid systems, *Int. J. Multiph. Flow.* 27 (2001) 885–910.
- [44] Y. Taitel, D. Bornea, A.E. Dukler, Modelling flow pattern transitions for steady upward gas-liquid flow in vertical tubes, *AIChE J* 26 (1980) 345–354.
- [45] D. Barnea, O. Shoham, Y. Taitel, A.E. Dukler, Gas-liquid flow in inclined tubes: Flow pattern transitions for upward flow, *Chem. Eng. Sci.* 40 (1985) 131–136.
- [46] S.E. Haaland, Simple and Explicit Formulas for the Friction Factor in Turbulent Pipe Flow, *J. Fluids Eng* 105 (1983) 89–90.
- [47] A.E. Dukler, M.G. Hubbard, A Model for Gas-Liquid Slug Flow in Horizontal and Near Horizontal Tubes, *Ind. Eng. Chem. Fundam.* 14 (1975) 337–347.
- [48] K.H. Bendiksen, D. Maines, R. Moe, S. Nuland, The Dynamic Two-Fluid Model O.L.G.A.: Theory and Application, *SPE Prod. Eng.* 6 (1991) 171–180.
- [49] G.A. Gregory, M.K. Nicholson, K. Aziz, Correlation of the liquid volume fraction in the slug for horizontal gas-liquid slug flow, *Int. J. Multiph. Flow.* 4 (1978) 33–39.
- [50] G.B. Wallis, *One-Dimensional Two-Phase Flow*, Mc Graw-Hill, New York, 1969.
- [51] R.V.A. Oliemans, B.F.M. Pots, N. Trompé, Modelling of annular dispersed two-phase flow in vertical pipes, *Int. J. Multiph. Flow.* 12 (1986) 711–732.